Journal of Biomolecular NMR
https://doi.org/10.1007/s10858-017-0160-3

ARTICLE

# Stable and rigid DTPA-like paramagnetic tags suitable for in vitro and in situ protein NMR analysis

Jia-Liang Chen[1] · Yu Zhao[1] · Yan-Jun Gong[1] · Bin-Bin Pan[1] · Xiao Wang[1] · Xun-Cheng Su[1]

Received: 9 October 2017 / Accepted: 5 December 2017


## Abstract

Organic synthesis of a ligand with high binding affinities for paramagnetic lanthanide ions is an effective way of generating paramagnetic effects on proteins. These paramagnetic effects manifested in high-resolution NMR spectroscopy are valuable dynamic and structural restraints of proteins and protein–ligand complexes. A paramagnetic tag generally contains a metal chelating moiety and a reactive group for protein modification. Herein we report two new DTPA-like tags, 4PS-PyDTTA and 4PS-6M-PyDTTA that can be site-specifically attached to a protein with a stable thioether bond. Both protein-tag adducts form stable lanthanide complexes, of which the binding affinities and paramagnetic tensors are tunable with respect to the 6-methyl group in pyridine. Paramagnetic relaxation enhancement (PRE) effects of Gd(III) complex on protein-tag adducts were evaluated in comparison with pseudocontact shift (PCS), and the results indicated that both 4PS-PyDTTA and 4PS-6M-PyDTTA tags are rigid and present high-quality PREs that are crucially important in elucidation of the dynamics and interactions of proteins and protein-ligand complexes. We also show that these two tags are suitable for in-situ protein NMR analysis.

**Keywords** Paramagnetic NMR · Protein ligation · Paramagnetic tag · PRE · PCS

## Introduction

Paramagnetic effects manifested in high-resolution NMR spectroscopy provide rich sources of structural and dynamic restraints of proteins. These paramagnetic effects are generally termed as pseudocontact shift (PCS), paramagnetic relaxation enhancement (PRE), and residual dipolar couplings (RDCs) (Bertini et al. 2002; Otting 2010; Clore and Iwahara 2009; Koehler and Meiler 2011; Hass and Ubbink 2014). Paramagnetic NMR spectroscopy is a sensitive and efficient biophysical method in analysis of protein structures and interactions. Recently, it has been applied in structure determinations of protein–protein/ligand complexes (Hass and Ubbink 2014; Pintacuda et al. 2006; Tang et al. 2006; John et al. 2006; Saio et al. 2011; Guan et al. 2013), and elucidating the conformational replacement of multi-domain proteins (Bertini et al. 2004, 2010, 2012; Tang et al. 2007; Russo et al. 2013; Chen et al. 2016a, b; Fragai et al. 2013; Saio et al. 2015; Camilloni and Vendruscolo 2015; Luchinat 2016). As PCS can be determined readily and quantitatively in short time, it was applied as structural restraints in 3D structure determination of an unstable and low-abundance enzyme intermediate in real-time reaction system (Chen et al. 2016).

Since many proteins do not have a paramagnetic center, site-specific labeling proteins with a paramagnetic tag is generally required to achieve paramagnetic effects. Lanthanide ions are most preferable paramagnetic ions in paramagnetic NMR spectroscopy because of the diverse paramagnetic properties and similar coordination chemistry among the lanthanide series (Bertini et al. 2002; Pintacuda et al. 2007). Strategies of anchoring a paramagnetic ion in a protein have been proposed (Su and Otting 2010; Liu et al. 2014a, b; Nitsche and Otting 2017a), but most

Jia-Liang Chen and Yu Zhao have contributed equally.

**Electronic supplementary material** The online version of this article (https://doi.org/10.1007/s10858-017-0160-3) contains supplementary material, which is available to authorized users.

✉ Xun-Cheng Su
xunchengsu@nankai.edu.cn

[1] State Key Laboratory of Elemento-Organic Chemistry and Collaborative Innovation Center of Chemical Science and Engineering (Tianjin), College of Chemistry, Nankai University, Tianjin 300071, China

Published online: 09 December 2017

efforts have been made for in-vitro NMR analysis. Recent studies of protein structures and interactions in cells or closed to the cellular environment (for example, crowding conditions) have received great interests (Barbieri et al. 2016; Luchinat and Banci 2016, 2017; Sarkar et al. 2013; Smith et al. 2015; Martorana et al. 2014; Yang et al. 2017; Hänsel et al. 2014; Li and Liu 2012; Plitzko et al. 2017; Ye et al. 2015). The in situ condition either in cells or in-cell like environment contains multiple cellular components or high concentration of crowding media that might affect the stability of protein-tag adduct, therefore, stable paramagnetic tag is required for in-situ paramagnetic NMR analysis of proteins (Pan et al. 2016; Hikone et al. 2016; Müntener et al. 2016). The linkage between the protein and a tag should be stable and resistant to high concentration of intracellular GSH. In addition, the tag should have a high-binding affinity for a metal ion, which retains the paramagnetic center tightly in protein-tag complex. To achieve a stable tether between the tag and a protein, several strategies have been proposed (Chen et al. 2016; Hikone et al. 2016; Liu et al. 2014a, b; Yang et al. 2013, 2015; Li et al. 2012; Loh et al. 2013, 2015; Jiang et al. 2017). PCS analysis of protein samples in crowding conditions was firstly reported by using a stable 4-vinyl(pyrid ine-2,6-diyl)bis-methylenenitrilo tetrakis-(acetic acid) (4VPyMTA) tag (Yang et al. 2013), and the stable PyMTA tags allowed one to determine the protein structure in living cells with PCS data (Pan et al. 2016). 1,4,7,10-Tetraazacyclododecane-*N,N′,N″,N‴*-tetraacetic acid (DOTA) derivatives were also reported to measure PCS of proteins in living cells (Hikone et al. 2016; Müntener et al. 2016), albeit few PCSs were determined in HeLa cells. Since few paramagnetic tags have been reported for in situ NMR analysis (Pan et al. 2016; Hikone et al. 2016; Müntener et al. 2016; Yang et al. 2013), comparison of paramagnetic effects on proteins in different crowding media has to be evaluated and high-quality tags suitable for in situ NMR analysis are highly demanded.

The derivatives of ethylene diamine tetraacetic acid (EDTA) are widely used in NMR analysis because of the high binding affinity for lanthanide ions (Gaponenko et al. 2002; Ikegami et al. 2004; Leonov et al. 2005; Peters et al. 2011), but multiple chiral forms are produced upon coordination with metal ions. The optically purified ligand is thus generally required for paramagnetic NMR analysis (Leonov et al. 2005; Peters et al. 2011). Similar to EDTA, PyMTA tags have very high binding affinities for lanthanide ions ($10^{-18}$ to $10^{-19}$ mol $L^{-1}$) (Pellegatti et al. 2008) and have been used successfully in crowded conditions and in living cells (Pan et al. 2016; Yang et al. 2013). Derivatives of DOTA-like tags also form very stable and kinetic-inert complexes with lanthanides and have been extensively applied as stable paramagnetic tags (Hikone et al. 2016; Keizers et al. 2007, 2008; Häussinger et al. 2009; Liu et al. 2012; Graham et al. 2011; Lee et al. 2015; Yang et al. 2016).

Diethylene triamine pentaacetic acid (DTPA) has high binding affinities for lanthanides ($10^{-22}$ mol $L^{-1}$) (Pettit and Powell 1999), but its derivatives for tagging proteins are less studied in comparison with EDTA, PyMTA, and DOTA derived tags (Jiang et al. 2017; Prudêncio et al. 2004). The challenge of DTPA-like tags for site-specific labeling proteins is to prevent from the generation of new chiral centers upon binding to a metal ion. An advantage of polyamine carboxylate tags, including PyMTA, DTPA and TAHA, over DOTA-like tag is the ready preparation of protein-tag-Ln complexes by titrating the protein-tag sample with metal ions, which avoids multistep preparations of protein-tag-Ln adduct in one ligation per one metal ion. In the present study, we report two new DTPA-like paramagnetic tags, 2,2′,2″,2‴-((((4-phenylsulfonyl)pyridine-2-yl)methyl)azanediyl)bis(ethane-2,1-diyl)bis (azanetriyl)tetraacetic (4PS-PyDTTA) and 2,2′,2″,2‴-(((4-(phenylsulfonyl)pyridine-2-2yl)methyl)azanediyl)bis(ethane-2,1-diyl)bis(azanetriyl) tetraacetic acid (4PS-6M-PyDTTA, where 6M represents the 6-mehtyl group in pyridine) (Fig. 1). Both two tags were efficiently attached to a protein via formation of a stable thioether bond between the tag and a protein. The performance of these DTPA-like protein conjugates has been evaluated by paramagnetic NMR spectroscopy in vitro and in different crowding media including Ficoll, BSA and *E. coli* cell lysate.

## Experimental section

### Synthesis of tag 4PS-PyDTTA

Compounds **2**–**6** and **12** were synthesized as previously reported (Ding et al. 2011; Ochiai 1953; Kmentova et al. 2010; Yuan and Guo 2011).

2,2′-((((4-(Phenylsulfonyl)pyridin-2-yl)methyl)azanediyl)bis(ethane-2,1-diyl))bis(isoindoline-1,3-dione) (**7**). Under argon atmosphere, compound **6** (1.0 g, 3.75 mmol), **12** (2.2 g, 6.0 mmol), $K_2CO_3$ (4.0 g, 29.0 mmol) and KI (0.2 g, 1.2 mmol) were mixed with 120 mL acetonitrile

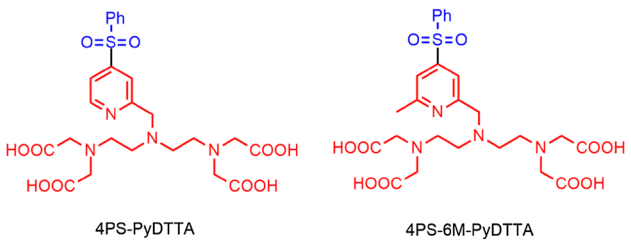


**Fig. 1** Structures of DTPA-like tags, 4PS-PyDTTA and 4PS-6M-PyDTTA

(Miranda et al. 2004). The reaction mixture was stirred at room temperature for 1 h, and was then refluxed at 80 °C for 10 h. The filtrate was concentrated and purified by silicon column to obtain **7** (1.1 g, 49.5%) as yellow solid. $^{1}$H-NMR (400 MHz, $CDCl_3$) $\delta$ ppm: 8.58 (1H, s), 7.98 (1H, s), 7.96 (1H, d, J = 1.42 Hz), 7.82 (1H, s), 7.74–7.66 (8H, m), 7.57 (1H, t, J = 7.40 Hz), 7.53–7.48 (3H, m), 3.95 (2H, s), 3.76 (4H, t, J = 6.36 Hz), 2.88 (4H, t, J = 6.20 Hz).

$N^1$-(2-Aminoethyl)-$N^1$-((4-(phenylsulfonyl)pyridin-2-yl)methyl) ethane-1,2-diamine (**8**). Following the similar procedure as published previously (Anderson et al. 2001), 1.2 mL (10.38 mmol) 80% drazine hydrate was added dropwise to a solution of **7** (1.0 g, 1.68 mmol) in 30 mL methanol. The reaction mixture was refluxed at 70 °C for 13 h. Then the mixture was filtered and the solvent was removed under reduced pressure to obtain **8** (0.35 g, 62.5%) as yellow oil. $^{1}$H-NMR (400 MHz, $CDCl_3$) $\delta$ ppm: 8.74 (1H, d, J = 5.12 Hz), 8.02 (1H, s), 8.00 (1H, d, J = 1.44 Hz), 7.96 (1H, s), 7.69–7.64 (2H, m), 7.61–7.57 (2H, m), 3.87 (2H, s), 2.78 (4H, t, J = 6.08 Hz), 2.62 (4H, t, J = 6.08 Hz).

Tetraethyl 2,2′,2″,2‴-(((((4-(phenylsulfonyl)pyridin-2-yl)methyl) azanediyl)bis(ethane-2,1-diyl)) bis(azanetriyl))tetraacetate (**9**). Under argon atmosphere, 2.2 mL (16.72 mmol) ethyl 2-bromoacetate in 20 mL acetonitrile was added dropwise to a mixture of **8** (0.35 g, 1.05 mmol), $K_2CO_3$ (3.6 g, 26.3 mmol), KI (0.2 g, 1.2 mmol) and 25 mL acetonitrile. Then the reaction mixture was stirred at room temperature for 38 h, and filtered. The filtrate was concentrated and purified by silicon column to obtain **9** (0.39 g, 54.3%) as brown oil. $^{1}$H-NMR (400 MHz, $CDCl_3$) $\delta$ ppm: 8.67 (1H, d, J = 5.12 Hz), 8.03 (1H, d, J = 1.04 Hz), 8.00 (1H, s), 7.98 (1H, d, J = 1.44 Hz), 7.64–7.60 (1H, m), 7.59–7.54 (3H, m), 4.14 (8H, q, J = 7.12 Hz), 3.88 (2H, s), 3.52 (8H, s), 2.85 (4H, t, J = 6.48 Hz), 2.67 (4H, t, J = 7.64 Hz), 1.24 (12H, t, 7.16 Hz).

2,2′,2″,2‴-(((((4-(Phenylsulfonyl)pyridin-2-yl)methyl) azanediyl)bis(ethane-2,1-diyl))bis(azanetriyl))tetraacetic acid (4PS-PyDTTA). A mixture of **9** (0.35 g, 0.52 mmol), NaOH (0.12 g, 3.09 mmol), 5 mL ethanol and 5 mL water was stirred at room temperature overnight. The resulting mixture was treated with Dowex $H^+$ ion exchange resin to pH 4. The mixture was filtered and the filtrate was concentrated to obtain 4PS-PyDTTA (0.22 g, 75.9%) as pale yellow solid. $^{1}$H-NMR (400 MHz, 90% $H_2O$ + 10% $D_2O$) $\delta$ ppm: 8.67 (1H, d, J = 5.32 Hz), 7.98–7.94 (3H, m), 7.80 (1H, d, J = 5.08 Hz), 7.66 (1H, t, J = 7.12 Hz), 7.56 (2H, t, J = 7.68 Hz), 3.89 (2H, s), 3.62 (8H, s), 3.29 (4H, t, J = 6.41 Hz), 2.87 (4H, t, J = 6.02 Hz). $^{13}$C-NMR (100 MHz, 90% $H_2O$ + 10% $D_2O$) $\delta$ ppm: 169.89, 159.27, 150.81, 149.95, 137.55, 135.21, 130.04, 128.17, 120.98, 119.96, 57.63, 56.87, 52.36, 48.12. MS-ESI (+): 567.2.

### Synthesis of tag 4PS-6M-PyDTTA

Tag 4PS-6MPyDTTA was synthesized similar to 4PS-PyDTTA.

$^{1}$H-NMR (400 MHz, 90% $H_2O$ + 10% $D_2O$) $\delta$ ppm: 7.96 (2H, d, J = 7.92 Hz), 7.86 (1H, s), 7.74 (1H, s), 7.66 (1H, t, J = 7.52 Hz), 7.56 (2H, t, J = 8.12 Hz), 3.83 (2H, s), 3.59 (8H, s), 3.27 (4H, t, J = 6.96 Hz), 2.86 (4H, t, J = 6.88 Hz), 2.53 (3H, s). $^{13}$C-NMR (100 MHz, 90%$H_2O$ + 10%$D_2O$) $\delta$ ppm: 169.72, 160.91, 157.70, 151.91, 150.98, 137.40, 135.23, 130.00, 128.16, 121.61, 118.72, 57.30, 56.67, 52.10, 48.09, 22.66. MS-ESI (−): 579.2.

### Protein expression and purification

Uniformly $^{15}$N-labelled human ubiquitin S57C mutant and *Staphylococcus aureus* sortase A (SrtA) G167E/D82C mutant were prepared using an optimized high-density method (Cao et al. 2014) according to the previous protocol (Marley et al. 2001). Typically, 20 mg $^{15}$N-ubiquitin and 16 mg $^{15}$N-SrtA was produced from 250 mL M9 media.

### Site-specific labelling of proteins with DTPA-like tags

0.8 mM $^{15}$N-labelled protein in 20 mM tris(hydroxymethyl) aminomethane (Tris) and at pH 7.6 was first mixed with 1 equivalent tris(2-carboxyethyl)phosphine (TCEP) to restore the free sulfydryl group. Five equivalents of 4PS-PyDTTA or 4PS-6M-PyDTTA (50 mM as a stock in MilliQ water) were added to the protein solution, and the pH was adjusted to 8.5 using 1.0 M NaOH. The reaction mixture was incubated at room temperature for about 8–16 h. The ligation process was monitored by matrix-assisted laser desorption ionization-time of flight (MALDI-TOF) mass spectroscopy. The reaction product was purified with a small desalting PD10 column or through an anion exchange column with FPLC. Due to the unavoidable loss of proteins during purification, the overall yield was about 50–70%.

### NMR measurements

All NMR experiments were recorded at 298 K on a Bruker Avance 600 MHz spectrometer equipped with a QCI-cryoprobe unless described otherwise. All $^{15}$N-HQSC spectra were performed for 0.10 mM $^{15}$N-ubiquitin or 0.15 mM $^{15}$N-SrtA in 20 mM 2-(*N*-morpholino)ethanesulfonic acid (MES) buffer at pH 6.4. The 1D $^{1}$H-spectra were recorded for a solution of 1.0 mM 4PS-PyDTTA or 4PS-6M-PyDTTA in $D_2O$ at pD 7.0–8.0 with step-wise addition of lanthanide ion (in 100 mM stock solution) and no pD was adjusted during the titration. Paramagnetic or diamagnetic protein samples were prepared by titrating lanthanide ion (10 mM in stock solution) with the protein-tag solution up to the molar

ratio of [protein]/[metal ion] about 1:1.1. As to the sample of SrtA-tag, ethylene-diamine-tetraacetic acid (EDTA) up to 20% of protein-tag concentration was added to assure no excess of lanthanide ion was loaded to prevent the additional binding site of lanthanide in the calcium binding-motif in SrtA.

300 g/L stock solution of Ficoll and BSA were prepared in 20 mM MES at pH 6.4. The cell lysate was prepared as following. The *E. coli*. BL21(DE3) condon plus cells were grown at 37 °C in 20 mL Luria broth rich media shaken at 190 rpm for 5 h. The cells were harvested by centrifugation at 3000*g* for 8 min at 4 °C when the cell density at 600 nm ($OD_{600}$) reached about 0.8. The cell pellets were resuspended in 1 mL 20 mM MES buffer at pH 6.4 and sonicated on ice for 15 min. The cell lysates were obtained by centrifugation at 12000*g* for 5 min, and the supernatant was used as crowing media for NMR analysis.

### Calculation of the Δχ-tensors

The Δχ-tensors were determined using the Numbat program (Schmitz et al. 2008). Only PCS values of residues in secondary structural elements were used in the fit to the first conformer of NMR structures for ubiquitin (PDB: 2MJB) or the crystal structure of wide-type SrtA (PDB: 1T2P). Q-factors were calculated as following Eq. (1)

$$Q = \frac{\sqrt{\sum (PCS\_\exp - PCS\_calc)^2}}{\sqrt{\sum (PCS\_\exp)^2}} \quad (1)$$

where PCS_exp and PCS_calc are the experimental and back-calculated PCS data, respectively.

### RDC measurement and calculation of alignment tensors

RDC values of one bond $^1H$–$^{15}N$ $^1D_{NH}$ were recorded as the difference of $^{15}N$-doublet splitting between the paramagnetic and diamagnetic samples by using IPAP pulse sequence (Ottiger et al. 1998). Alignment tensors were calculated by using Module program (Dosset et al. 2001). Only RDCs of residues in secondary structural regions were used to calculate the alignment tensors. Q-factors were calculated as following Eq. (2)

$$Q = \frac{\sqrt{\sum (RDC\_\exp - RDC\_calc)^2}}{\sqrt{\sum (RDC\_\exp)^2}} \quad (2)$$

where RDC_exp and RDC_calc are experimental and back-calculated RDC values. The theoretical alignment tensors (A) were calculated from the Δχ-tensors based on the equation:

$$\Delta\chi_{ax,rh} = \frac{15\mu_0 kT}{B_0^2} A_{ax,rh} \quad (3)$$

where $B_0$ is the magnetic field strength, $\mu_0$ the induction constant, k the Boltzmann constant, and T the temperature.

## Results and discussion

The new DTPA-like tag contains a general DTPA metal chelating moiety and a thiol-reactive group, phenylsulfonated pyridine (Yang et al. 2015), which is attached to the central nitrogen in the DTPA-backbone chain. The detailed synthesis is shown in Scheme 1. Starting from commercially available materials, the two tags were achieved via 10-step synthesis with the overall yield of about 2 and 3%, respectively.

4PS-PyDTTA and 4PS-6M-PyDTTA have similar chelating atoms as DTPA (Fig. 1) and one expects that the pyridine nitrogen could bind to the metal ion. In addition, the methyl group in 4PS-6M-PyDTTA might influence the stability and rigidity of metal complex in the protein-tag adducts.

### Site-specific labeling of proteins with DTPA-like tags

1D proton NMR spectroscopy indicated that both tags have high selectivity towards the thiol group of L-cysteine (data not shown). The reactivity of 4PS-PyDTTA and 4PS-6M-PyDTTA towards solvent exposed protein thiols was therefore assessed at pH 8.5 in 20 mM Tris buffer. Human ubiquitin S57C mutant and *Staphylococcus aureus* sortase A D82C/G167E mutant (SrtA D82C) were used as model proteins in this study. MALDI-TOF mass spectroscopy showed that the mass difference between the ligation product and free protein was in agreement with the theoretical mass difference (Scheme 2 and Fig. 2). It is noted that the DTTA moiety in its protein adducts was partially broken during ionization as shown in Fig. 2, resulting in smaller molecular sizes than that of the protein-tag conjugate. The overall ligation yields were 70% for ubiquitin S57C and 50% for SrtA D82C, which were purified with desalting column and FPLC, respectively. 4PS-6M-PyDTTA has generally faster reaction rates than 4PS-PyDTTA in ligation with ubiquitin S57C and SrtA D82C, and the reaction completed within 8 h for both proteins. As to 4PS-PyDTTA, extended incubation time (~ 16 h) is required to achieve high-yield ligation product. The fact that lower reactivity of 4PS-PyDTTA than 4PS-6M-PyDTTA is consistent with the previous analysis (Martorana et al. 2015), which indicated that the methyl group at the sixth position of pyridine increases the reactivity of

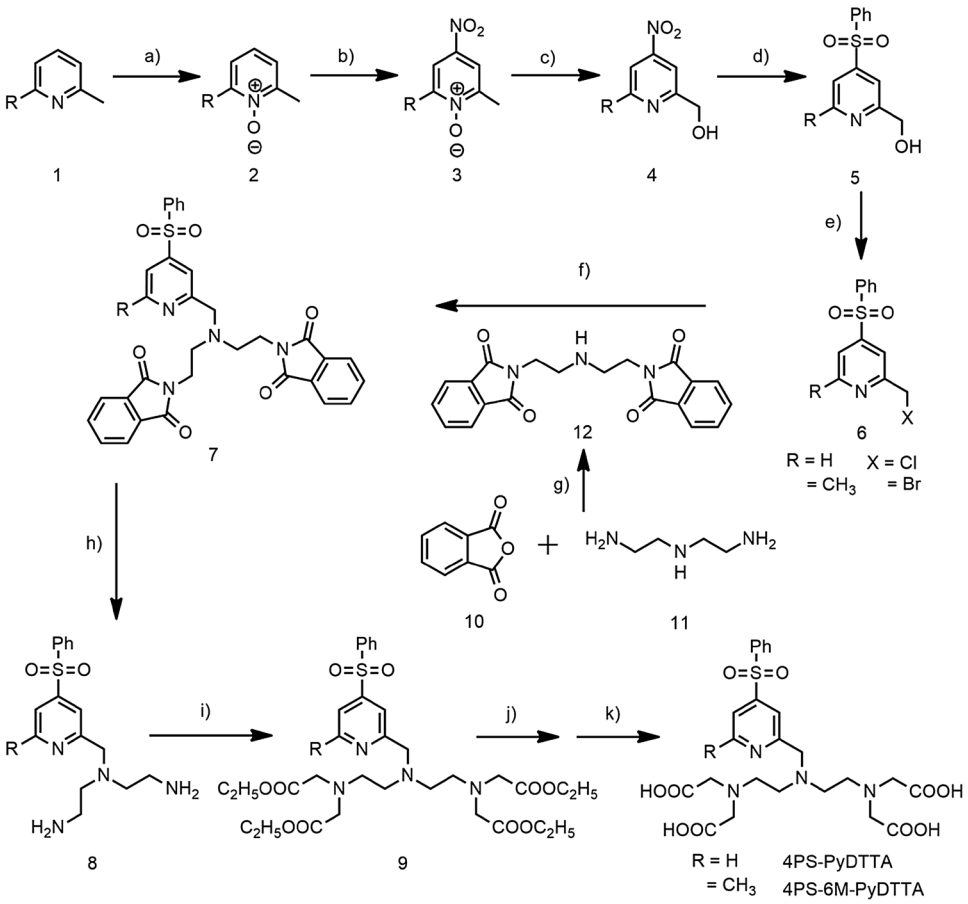


**Scheme 1** Synthesis of DTPA-like tags. (*a*) AcOH, $H_2O_2$; (*b*) $H_2SO_4$, $HNO_3$; (*c*) $(CF_3CO)_2O$, $CH_2Cl_2$; (*d*) $CH_3CN$, $PhSO_2Na$, Ar; (*e*) $SOCl_2$, $CH_2Cl_2$ for R=H; $PBr_3$, $CHCl_3$ for R=$CH_3$; (*f*) $CH_3CN$, KI, $K_2CO_3$, Ar; (*g*) HOAC; (*h*) $N_2H_4{\cdot}H_2O$, $CH_3OH$; (*i*) $BrCH_2CO_2C_2H_5$, $CH_3CN$, KI, $K_2CO_3$, Ar; (*j*) NaOH, $C_2H_5OH$, $H_2O$; (*k*) $H^+$

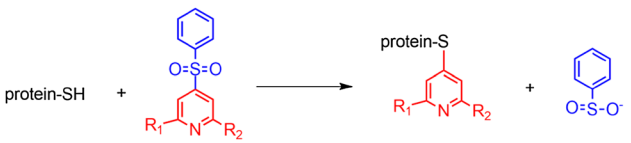


**Scheme 2** Site-specific tagging proteins via generation of a stable thioether bond between a protein and DTPA-like tags in aqueous solution

4-phenylsulfonated pyridine derivatives towards solvent exposed cysteines.

SrtA D82C mutant contains a native cysteine, C184, and it is the key residue for the enzyme activity. The MALDI-TOF experiment indicated that only one tag was attached to a single protein, suggesting one cysteine was modified with the tag. Chemical shift perturbation analysis indicated that the residues with large chemical shift changes in SrtA D82C-tag adducts were located near the residue D82C. In contrast, negligible chemical shift changes were observed for the residues close to C184, suggesting that these two tags only react with C82 but not C184 (Fig. S1).

We previously showed that the reactivity of a cysteine in a protein tightly correlates with its local chemical environment (Ma et al. 2014), which can be applied for site-specific tagging a protein containing more than one cysteines with a single paramagnetic tag. Using PyMOL program (http://www.pymol.org), the solvent accessibility of cysteine side chains was determined for C82 and C184 in SrtA, and S57C in ubiquitin. The calculated solvent accessible surface area (SASA) of side chain C82 in SrtA and S57C in ubiquitin was 62.2 and 102.9 $Å^2$, respectively. However, the SASA of C184 side chain in SrtA is only 2.4 $Å^2$, which prevents from the reaction with phenylsulfonated pyridine tags.

## Interaction of DTPA-like tags with lanthanide ions

The interactions of 4PS-PyDTTA and 4PS-6M-PyDTTA with lanthanide ions were analyzed with 1D proton NMR spectroscopy. Addition of diamagnetic $Y^{3+}$ into the solution of DTPA-like tag produced new proton signals, while the peak intensity of free tags decreased gradually. The new NMR signals experienced no further changes till the molar ratio of [tag]/[$Y^{3+}$] 1:1 was reached, indicating the tag form a 1:1 complex with $Y^{3+}$ (Fig. S2). Paramagnetic $Ce^{3+}$, $Yb^{3+}$, and $Tm^{3+}$ generated well dispersed NMR signals in complex with the new tags (Fig. S2). Notably, more paramagnetic NMR signals were determined in the complexes

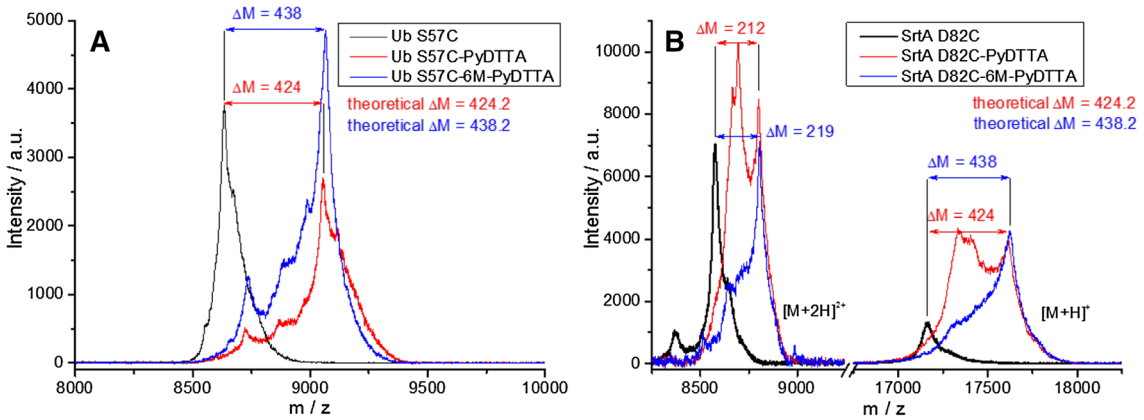


**Fig. 2** MALDI-TOF mass spectra of ubiquitin S57C (**a**) and SrtA D82C (**b**) before and after ligation with 4PS-PyDTTA and 4PS-6M-PyDTTA tags. Mass spectra of free ubiquitin S57C and SrtA D82C are shown in black. The red and blue spectra were recorded for the mixture of 0.1 mM protein with 0.4 mM 4PS-PyDTTA (red) or 4PS-6M-PyDTTA (blue) after incubation for 12 h in 20 mM Tris–HCl buffer, pH 8.5, and 0.1 mM TCEP. The molecular mass is indicated and the mass difference between protein-tag and protein is in agreement with the theoretical mass differences for ligation with a single tag molecule mass difference between ligation

of 4PS-6M-PyDTTA than in those of 4PS-PyDTTA. In addition, the former complexes presented overall narrower NMR signals (Fig. S2). These results suggest that the methyl group in 4PS-6M-PyDTTA might restrict the conformation averaging in the metal complex and more experiments were performed in the protein-tag adducts.

## Binding affinity assessment of protein-PyDTTA/6M-PyDTTA adduct with lanthanide ions

To assess the binding affinity of protein-PyDTTA/6M-PyDTTA adduct with lanthanide ions, we performed the competition affinity measurement by addition of a strong lanthanide binding ligand, EDTA, into the mixture of protein-PyDTTA/6M-PyDTTA and metal ion. Addition of one equivalent EDTA to the mixture of 0.1 mM ubiquitin S57C-PyDTTA (or 6M-PyDTTA) and 0.1 mM $Tm^{3+}$ in 20 mM MES at pH 6.4 produced negligible changes in cross-peak intensities for the paramagnetic species in the $^{15}$N-HSQC spectra. Five equivalents of EDTA only resulted 20% decrease in the peak intensity in ubiquitin-6M-PyDTTA-Tm complex, whereas the spectrum of ubiquitin-PyDTTA-Tm complex remained essentially unchanged. Further addition of EDTA gradually attenuated the cross-peak intensities of paramagnetic species for the samples of ubiquitin-6M-PyDTTA-Ln complexes (Fig. S3). The results showed that ubiquitin-PyDTTA and ubiquitin-6M-PyDTTA adducts present higher binding affinities for lanthanide ions than EDTA, but protein-PyDTTA binds metal ions stronger than protein-6M-PyDTTA.

In contrast to ubiquitin, SrtA contains a calcium binding motif that also binds lanthanide ions. Hence, selective

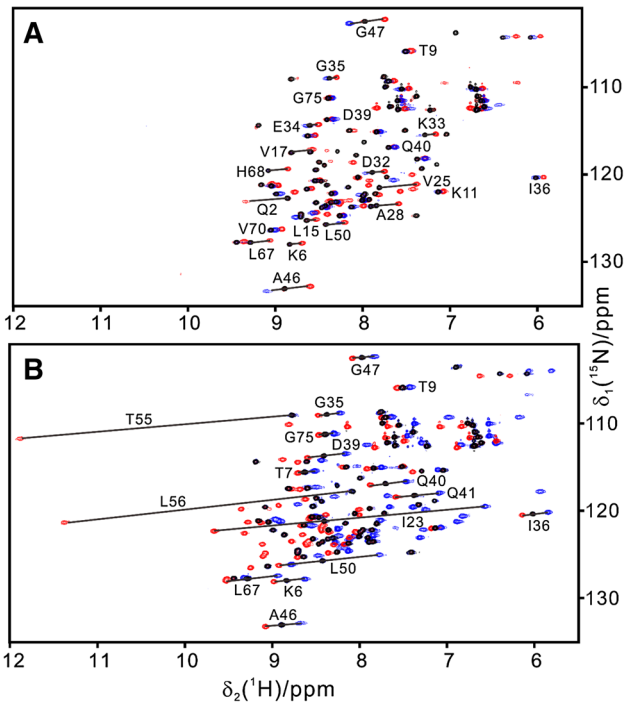


**Fig. 3** Superimposition of $^{15}$N-HSQC spectra of 0.10 mM $^{15}$N-ubiquitin S57C-tag in complex with one equivalent of $Y^{3+}$ (black), $Tm^{3+}$ (red), and $Tb^{3+}$ (blue), respectively. **a** Ubiquitin S57C-PyDTTA; **b** ubiquitin S57C-6M-PyDTTA

binding of SrtA-tag for lanthanide ions is required in design of a paramagnetic tag. Similar competition experiment was performed on the samples of SrtA D82C-PyDTTA-Ln and SrtA D82C-6M-PyDTTA-Ln with addition of EDTA. In the SrtA D82C-tag adducts, both PyDTTA and 6M-PyDTTA

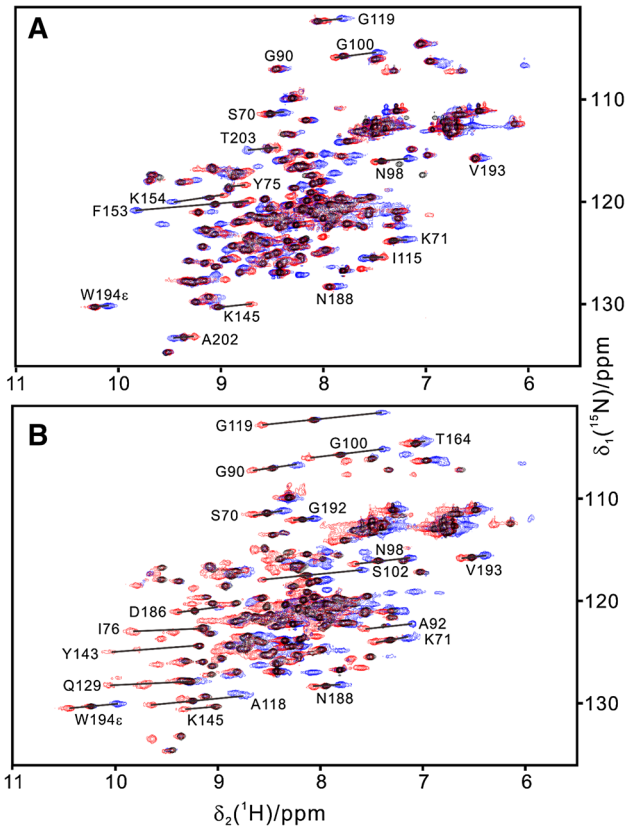


**Fig. 4** Superimposition of $^{15}$N-HSQC spectra of 0.15 mM $^{15}$N-SrtA D82C-tag in complex with one equivalent of $Y^{3+}$ (black), $Tm^{3+}$ (red), and $Tb^{3+}$ (blue), respectively. **a** SrtA D82C-PyDTTA; **b** SrtA D82C-6M-PyDTTA

bind lanthanide ions more tightly than the calcium binding motif. Similarly, SrtA D82C-PyDTTA has higher binding affinities for lanthanide ions than EDTA and preserves similar association constants as ubiquitin S57C-PyDTTA adduct (Fig. S4). As to the SrtA D82C-6M-PyDTTA-Tb complex, only 25% of paramagnetic species remained after addition of two equivalents of EDTA (Fig. S4) and four-fold excess of EDTA released all the bound $Tb^{3+}$ from the 6M-PyDTTA moiety in the SrtA-tag adduct, resulting in the diamagnetic protein.

To assess the protein local structure effects on the stability of protein-tag-Ln complex, we used PyDTTA analogue, the reaction products of DTT with 4PS-PyDTTA and 4PS-6M-PyDTTA, to compare the binding affinity for lanthanide with protein-tag conjugate. The reason is that the 4PS-PyDTTA/4PS-6M-PyDTA tags contain a phenylsulfonyl group, which is electron-withdrawing and decreases the coordinating ability of pyridine nitrogen to metal ions. The PyDTTA analogues resemble more similar chemical properties as the protein-tag adduct, and were therefore prepared by incubating the mixture of 0.5 mM 4PS-PyDTTA or 4PS-6M-PyDTTA and 2 mM DTT at pH 6.6 for 5 h without further purification. The complex of PyDTTA analogue and $Yb^{3+}$ is highly stable even in the presence of ten equivalents of EDTA. In contrast, the 6M-PyDTTA analogue presents similar binding affinity as EDTA for $Yb^{3+}$, since one equivalent of EDTA attenuated the NMR signals of 6M-PyDTTA analogue and $Yb^{3+}$ complex significantly and less than 20% complex was maintained when five equivalents of EDTA was added (Fig. S5). Similarly, the protein-PyDTTA adducts showed slightly higher affinities for lanthanide ions than the PyDTTA analogue (Figs. S5, S6). In contrast, the complex of ubiquitin S57C-6M-PyDTTA-Ln is more stable than that

**Table 1** $\Delta\chi$-Tensor parameters generated by different lanthanide ions in the protein-PyDTTA or 6M-PyDTTA complexes

| Protein | $N_{data}$ [a] | $Ln^{3+}$ | $\Delta\chi_{ax}$ [b] | $\Delta\chi_{rh}$ [b] | $\alpha$ [c] | $\beta$ [c] | $\gamma$ [c] | Q (%) |
|---|---|---|---|---|---|---|---|---|
| Ubiquitin-PyDTTA | 34 | Yb | 2.0 | 0.7 | 62.4 | 98.6 | 139.8 | 9.0 |
| | 34 | Tm | 6.5 | 1.3 | 57.5 | 101.7 | 147.6 | 5.6 |
| Ubiquitin-6M-PyDTTA | 34 | Yb | 3.6 | 0.2 | 131.4 | 105.8 | 68.9 | 6.4 |
| | 33 | Tm | 7.6 | 1.1 | 130.6 | 101.8 | 57.1 | 3.8 |
| | 32 | Tb | −10.5 | −1.7 | 132.1 | 106.6 | 67.8 | 3.3 |
| | 33 | Dy | −13.6 | −2.9 | 130.5 | 106.0 | 75.8 | 3.3 |
| SrtA-PyDTTA | 40 | Tm | 7.6 | 3.0 | 82.3 | 110.0 | 147.3 | 7.2 |
| | 29 | Tb | 14.3 | 4.1 | 6.9 | 52.8 | 166.3 | 5.8 |
| SrtA-6M-PyDTTA | 41 | Tm | 11.0 | 3.5 | 104.3 | 71.6 | 17.4 | 4.2 |
| | 28 | Tb | −14.3 | −4.8 | 106.2 | 72.0 | 23.6 | 6.9 |

The tensor parameters were obtained by fitting PCS data of backbone amide proton in the secondary structural elements to the NMR structure of ubiquitin (PDB code: 2MJB) (Maltsev et al. 2014) and crystal structure of SrtA (PDB code: 1T2P) (Zong et al. 2004)

[a] $N_{data}$ is the number of PCS values applied to calculate the paramagnetic tensor

[b] In units of $10^{-32}$ $m^3$

[c] In degrees relative to the reference structure

of 6M-PyDTTA analogue, whereas SrtA D82C-6M-PyDTTA presents similar affinity for the lanthanide ion as the 6M-PyDTTA analogue.

Taken together, our data showed that the stability of 4PS-PyDTTA and 4PS-6M-PyDTTA with lanthanide complex is high, but differ greatly with respect to presence of 6-methyl group in pyridine. Notably, the local protein structural environment at the ligation site also affects the stability of protein-tag-Ln complexes. These effects might stem from the formation of a rigid and compact tag-lanthanide moiety that interferes with the local protein structure, and such overall structural rearrangements in turn compromise the stability

**Table 2** Alignment tensor parameters generated by different lanthanide ions in the protein-PyDTTA or 6M-PyDTTA complexes

| Protein | $N_{data}$[a] | $Ln^{3+}$ | $A_{ax}$ ($\times 10^4$)[b] | $A_{rh}$ ($\times 10^4$)[b] | $\alpha$[c] | $\beta$[c] | $\gamma$[c] | Q (%) |
|---|---|---|---|---|---|---|---|---|
| Ubiquitin-PyDTTA | 34 | Yb | 0.5 (0.5) | 0.1 (0.2) | 135.6 | 102.0 | 169.4 | 47.3 |
| | 34 | Tm | 1.2 (1.7) | 0.6 (0.3) | 119.0 | 114.1 | 162.8 | 28.3 |
| Ubiquitin-6M-PyDTTA | 33 | Yb | 0.8 (0.9) | 0.3 (0.1) | 148.7 | 134.5 | −149.0 | 30.0 |
| | 30 | Tm | 1.6 (2.0) | 0.6 (0.3) | 156.5 | 133.4 | −146.3 | 26.3 |
| SrtA-PyDTTA | 25 | Tb | 2.5 (3.7) | 1.2 (1.1) | −86.5 | 130.3 | −81.8 | 32.4 |
| SrtA-6M-PyDTTA | 14 | Tb | −3.4 (−3.7) | −0.3 (−1.2) | 162.5 | 79.1 | −164.8 | 30.0 |

The tensor parameters were obtained by fitting RDC data of backbone amide protons in the secondary structural elements to the NMR structure of ubiquitin (PDB code: 2MJB) (Maltsev et al. 2014) or crystal structure of SrtA (PDB code: 1T2P) (Zong et al. 2004). All RDCs were measured at 298 K and 600 MHz $^1$H NMR frequency

[a]$N_{data}$ is the number of RDC values used to fit tensor

[b]Values in brackets were obtained from $\Delta\chi$-tensors using the Eq. (3), where $B_0$ is the magnetic field strength, $\mu_0$ the induction constant, k the Boltzmann constant, and T the temperature

[c]In degrees relative to the reference structure

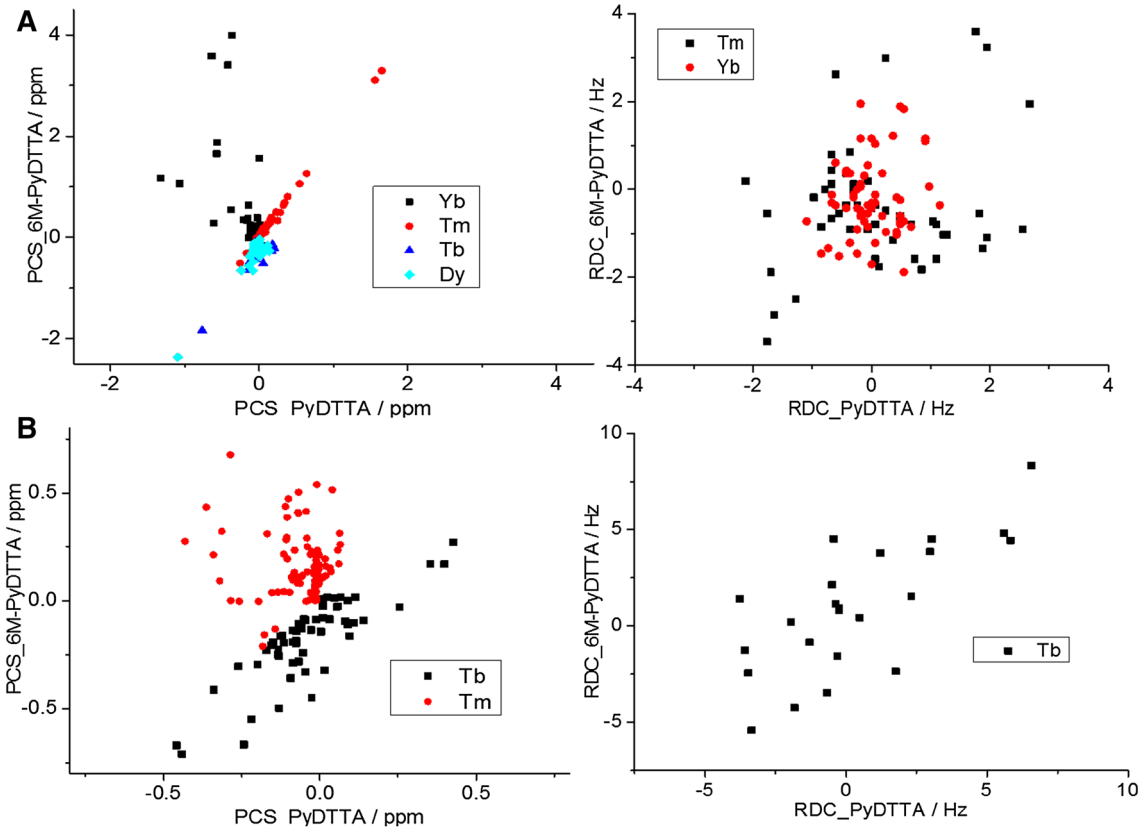


**Fig. 5** Comparison of PCSs and RDCs generated by lanthanide ions complexed with ubiquitin S57C-PyDTTA and ubiquitin S57C-6M-PyDTTA (**a**), and SrtA D82C-PyDTTA and SrtA D82C-6M-PyDTTA (**b**), respectively

of tag-lanthanide complex. Therefore, one needs to consider local structural effects of a protein on the stability of protein-tag metal complex in selection of a ligation site. To achieve this goal, computational design might be an ideal option (Nitsche et al. 2017b).

## PCS measurement and Δχ-tensor analysis

Ubiquitin S57C mutant was site-specifically labeled with PyDTTA and 6M-PyDTTA, respectively, in high yield. Paramagnetic samples were made by addition of $Yb^{3+}$, $Tm^{3+}$, $Tb^{3+}$, and $Dy^{3+}$ into the solution of ubiquitin-tag conjugate, and $^{15}$N-HSQC spectra were recorded accordingly. PCSs were measured as the chemical shift differences of backbone amide protons between the paramagnetic and diamagnetic samples (Table S1–S3). Addition of paramagnetic $Tm^{3+}$ into the protein-tag solution produced large chemical shift perturbations, and only one set of paramagnetic peaks was observed for the lanthanide complexes of ubiquitin S57C-PyDTTA and S57C-6M-PyDTTA (Fig. 3). Remarkably, the $Tm^{3+}$ complexes of ubiquitin S57C-PyDTTA and S57C-6M-PyDTTA shifted the NMR cross-peaks in opposite directions, suggesting different paramagnetic tensors in these two protein-tag complexes. Largest PCS, − 1.33 ppm of D21, was determined for the complex of ubiquitin S57C-PyDTTA-Yb, whereas PCS of 1.73 ppm was determined for the residue of S20 in the ubiquitin S57C-6M-PyDTTA-Yb complex. However, many cross-peaks were broadened in the complex of ubiquitin S57C-PyDTTA-Dy. In contrast, the paramagnetic complex of S57C-6M-PyDTTA produced larger chemical shift perturbations and less line-broadening effects.

We showed that 4PS-PyDTTA and 4PS-6M-PyDTTA site-specifically reacted with one cysteine for SrtA D82C containing two free cysteines (Fig. 2). Similar to ubiquitin-PyDTTA complex, only one paramagnetic species was observed in the $^{15}$N-HSQC spectra of the SrtA D82C-tag-Ln complex. In contrast to ubiquitin S57C-PyDTTA-Ln, SrtA D82C-PyDTTA-Ln generated larger PCSs and no significant line-broadening effects on protein signals (Fig. 4). The lanthanide complexes of protein-PyDTTA/or 6M-PyDTTA adducts presented only one paramagnetic species in solution, indicating that the presence of only one dominant conformation in solution.

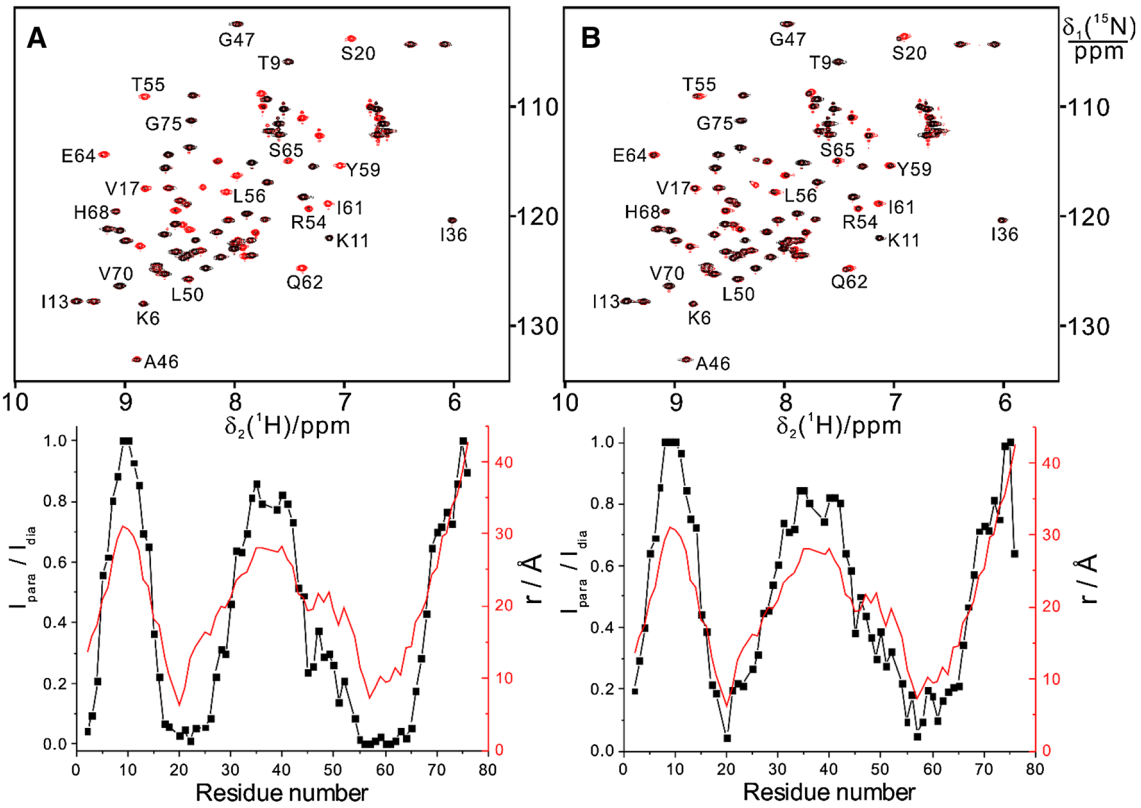


**Fig. 6** Comparison of PRE and PCS. **a** Ubiquitin-PyDTTA; **b** ubiquitin-6M-PyDTTA. The top panel shows the superimposition of $^{15}$N-HSQC spectra of ubiquitin S57C-tag in complex with one equivalent of $Gd^{3+}$ (black) and $Y^{3+}$ (red), respectively. The lower panel represents the correlation of cross-peak intensity $I_{para}/I_{dia}$ (left, black line) and the distance of the paramagnetic metal center from the backbone amide proton (right panel, red line) as a function of amino acid sequence, respectively. $I_{para}$ and $I_{dia}$ are the cross-peak intensities in HSQC spectra for the paramagnetic and diamagnetic samples, and the paramagnetic center was determined from Table 1

Paramagnetic Δχ-tensors were determined and the calculated Δχ-tensor parameters were listed in Table 1. Excellent correlation with small Q-factors between the observed and back-calculated PCSs suggested that the Δχ-tensors are reliable (Table 1 and Fig. S7). The calculated Δχ-tensors in ubiquitin adducts were similar to those of rigid Cys-Ph-TAHA tag complex, which was attached to ubiquitin S57C via a disulfide bond (Peters et al. 2011). The paramagnetic centers in ubiquitin-PyDTTA and ubiquitin-6M-PyDTTA were very close and had a distance of about 6.6 Å from the Cα atom of S57C. In contrast, the paramagnetic positions in the SrtA D82C-tag-Ln complexes vary significantly, in which the metal center has a distance of 6.4 and 9.0 Å from the Cα atom of D82C in SrtA D82C-PyDTTA and SrtA D82C-6M-PyDTTA, respectively (Fig. S8). The large variations in metal positions in SrtA-tag adducts might be caused by different structural orientations upon formation of the metal complex.

## Comparison of PCS and RDC

RDCs of protein backbone amides were measured for the complexes of ubiquitin-tag and SrtA-tag with paramagnetic lanthanide ions. RDC values were calculated as the differences of one bond $^{1}H–^{15}N$ coupling constant between the diamagnetic ($Y^{3+}$ as the reference) and paramagnetic species (Tables S4, S5). Largest RDC value, −2.68 Hz for D21 in the complex of ubiquitin S57C-PyDTTA-Yb and −3.04 Hz for Y59 was determined in the ubiquitin S57C-6M-PyDTTA-Yb complex. Larger RDC values, −6.57 Hz for G90 in SrtA D82C-PyDTTA-Tb and −5.42 Hz for A104 in SrtA D82C-6M-PyDTTA-Tb were determined, respectively. The RDC data are generally larger than those of stable and rigid ubiquitin G47C-PyMTA-Ln complexes, suggesting less conformational averaging in the protein-PyDTTA (or -6M-PyDTTA)-Ln complex.

The calculated alignment tensor parameters were shown in Table 2 (Fig. S9). Comparison of the alignment tensors determined from RDCs and back-calculated data from PCSs is informative to evaluate the rigidity of DTTA tag

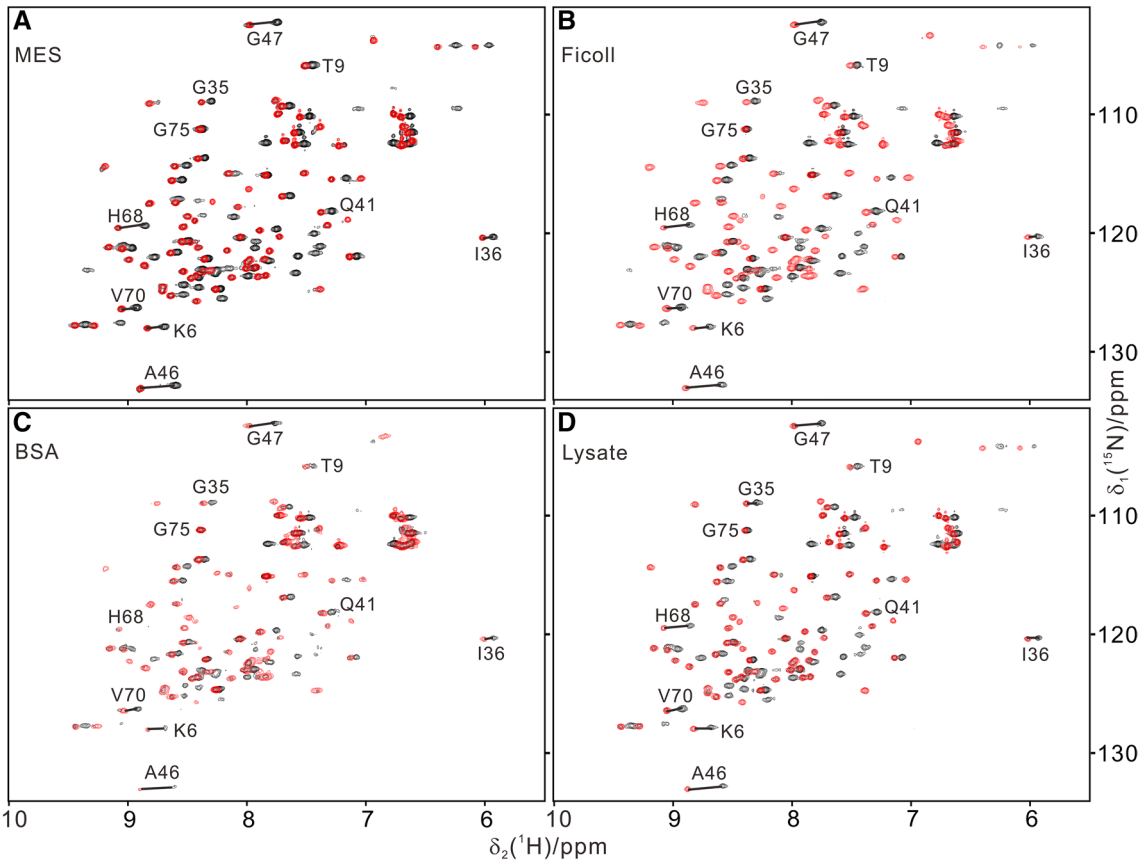


**Fig. 7** Superimposition of $^{15}N$-HSQC spectra recorded for 0.15 mM $^{15}N$-ubiquitin S57C-PyDTTA (red) and complexed with one equivalent of $Tm^{3+}$ (black) in different crowding media. **a** 20 mM MES buffer at pH 6.4; **b** 200 g/L Ficoll; **c** 100 g/L BSA; **d** *E. coli* cell lysate

with respect to the protein. The ratios of $A_{ax}$, the axial component of alignment tensor, calculated from RDCs and back-calculated from PCSs, were 0.7 and 0.8 for ubiquitin S57C-PyDTTA-Tm and S57C-6M-PyDTTA-Tm complexes, respectively (Table 2). These data are similar to the published values of very rigid DOTA-M8 tag complex (about 0.75) (Häussinger et al. 2009), and are also slightly larger than Cys-Ph-TAHA tag (ratio of 0.5) (Peters et al. 2011), of which all the paramagnetic tag were attached to ubiquitin S57C. As to SrtA, the $A_{ax}$ ratios are 0.7 and 0.9 for D82C-PyDTTA-Tb and D82C-6M-PyDTTA-Tb (Table 2), respectively. The determined $A_{ax}$ from RDCs in the protein-6M-PyDTTA-Ln complex was generally larger than that in the protein-PyDTTA-Ln complex as shown in Table 2, despite the varied paramagnetic centers from PCSs. Figure 5 presents the correlations of PCSs and RDCs determined from ubiquitin-tag and SrtA-tag complexes, indicating the lanthanide complexes of protein-PyDTTA and protein-6M-PyDTTA produced different paramagnetic $\Delta\chi$ tensors.

Since RDCs are independent of paramagnetic center, the overall larger alignment tensors from the lanthanide complex of 4PS-6M-PyDTTA protein conjugates indicate that the additional methyl group in pyridine not only alters the binding affinity for metal ions but also restricts the mobility of formed complex. This hypothesis is supported by the PCSs analysis, which showed that PCSs in protein-6M-PyDTTA-Ln complexes are generally larger than those in protein-PyDTTA-Ln complexes (Figs. 3, 4). These results of PCSs and RDCs are in excellent agreement with the data from EPR measurement in double electron–electron resonance (DEER) experiment, of which showed narrower distance distributions in the metal complex of protein-6M-PyEDTA than that of protein-PyEDTA (Martorana et al. 2015). Based on the crystal structure of DTPA-Y complex (Wang et al. 2000), similar structures of PyDTTA and 6M-PyDTTA with $Y^{3+}$ complexes were made (Fig. S10). It is evident that the complex of 6M-PyDTTA with $Y^{3+}$ represents a bulky structural view due to the presence of a methyl group at the sixth position in pyridine. This methyl group very likely restricts the reorientation of paramagnetic center in the 6M-PyDTTA complex but also decreases the stability of metal complex due to the steric repulsion as a compromise, which is absent from the PyDTTA-Y complex.

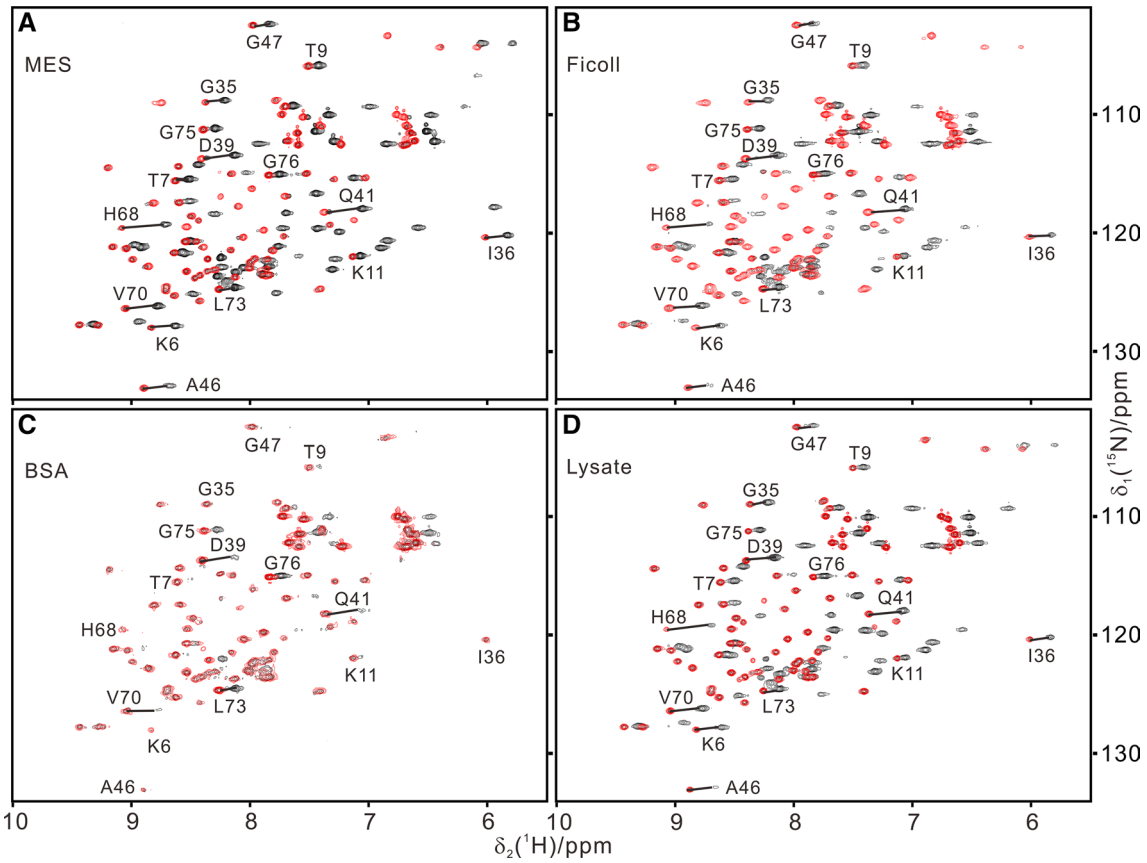


**Fig. 8** Superimposition of $^{15}$N-HSQC spectra recorded for 0.15 mM $^{15}$N-ubiquitin S57C-6M-PyDTTA (red) and complexed with one equivalent of $Tm^{3+}$ (black) in different crowding media. **a** 20 mM MES buffer at pH 6.4; **b** 200 g/L Ficoll; **c** 100 g/L BSA; **d** *E. coli* cell lysate

## PRE assessment of ubiquitin-PyDTTA adducts

PRE effects are valuable tools in evaluation of protein dynamics and interactions, however, these sensitive effects have to be regarded wisely and accurately. This is because any non-specific association of paramagnetic tag or free metal ion encountering to the protein surface will cause PREs in addition to the target interactions. Ubiquitin has a hot-spot surface that interacts with a large number of proteins (Lange et al. 2008; Perica and Chothia 2010), and it presents the challenge in optimization of a high-quality tag for both PRE and PCSs analysis. In recent years, we found that ubiquitin is an excellent model protein to assess the quality and rigidity of paramagnetic tags in development of high-quality tags. Herein, PRE values were measured for ubiquitin S57C-tag-$Gd^{3+}$ complexes for comparison with PCSs. Figure 6 presents the comparison of $^{15}$N-HSQC spectra for the samples of ubiquitin-tag in the presence of one equivalent diamagnetic $Y^{3+}$ and paramagnetic $Gd^{3+}$, respectively (Fig. 6). The correlation of cross-peak intensities as a function of amino acid sequence, as well as the back-calculated PREs attenuation from the paramagnetic center determined from PCSs, was evaluated. In Fig. 6, it was evident that the PREs effect on the cross-peak intensities correlated closely with the distance of backbone amide protons from the paramagnetic center (also Fig. S11). It suggested that the non-specific association of PyDTTA-Gd(III) complex with protein surface is negligible especially for most of the C-terminal flexible amino acids and the hot-spot patch including residues Leu8, Ile 44 and Val70 (Perica and Chothia 2010).

## Paramagnetic NMR analysis of proteins in crowding conditions

To evaluate the performance of paramagnetic tags in crowding media and further potential application for in-cell NMR analysis, different crowding media, including Ficoll, bovine serum albumin (BSA) and *E. coli* cell lysate, was used in this study. The stability of protein-PyDTTA (or 6M-PyDTTA) conjugate in complex with paramagnetic lanthanide ions was assessed in 200 g/L Ficoll, 100 g/L BSA and *E. coli* cell lysate, respectively. Because high concentration of BSA (200 g/L) broadens the NMR signals of ubiquitin, 100 g/L BSA in 20 mM MES buffer was used. The ubiquitin S57C-PyDTTA-Ln complexes presented similar $^{15}$N-HSQC spectra in these three crowding media as in vitro (Fig. 7), and

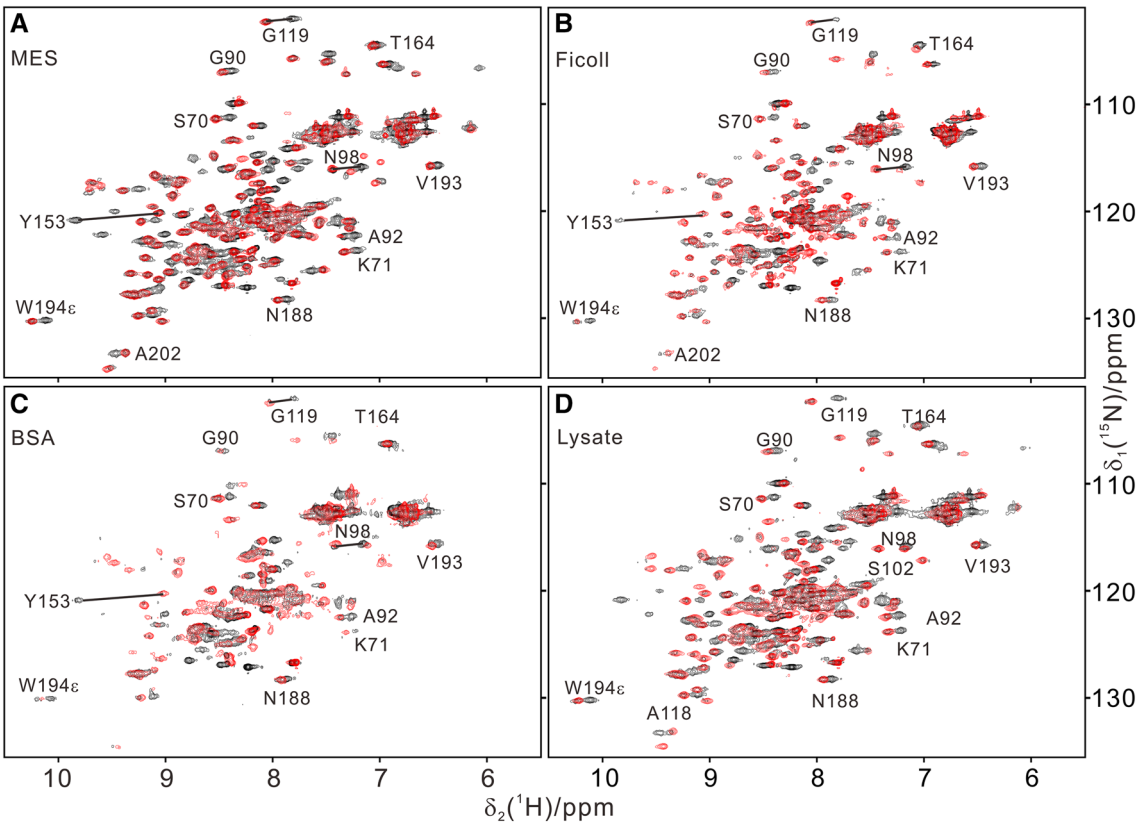


**Fig. 9** Superimposition of $^{15}$N-HSQC spectra recorded for 0.15 mM $^{15}$N-SrtA D82C-PyDTTA (red) and complexed with one equivalent of $Tb^{3+}$ (black) in different crowding media. **a** 20 mM MES buffer at pH 6.4; **b** 200 g/L Ficoll; **c** 100 g/L BSA; **d** *E. coli* cell lysate

the determined PCSs were almost identical to those from the in vitro samples. In contrast, the complex of ubiquitin S57C-6M-PyDTTA-Tb complex presented fewer cross-peaks in the $^{15}$N-HSQC spectra in 100 g/L BSA, but similar NMR spectra in 200 g/L Ficoll and the *E. coli*. cell lysate as in vitro (Fig. 8). As to the protein sample of SrtA D82C-PyDTTA-Tb complex, high-quality $^{15}$N-HSQC spectra were reproduced in 200 g/L Ficoll and the *E. coli* cell lysate but significant line-broadening effects were observed in 100 g/L BSA crowding media (Fig. 9). Notably, SrtA D82C-6M-PyDTTA-Tb complex in the three crowding media failed to reproduce high-quality $^{15}$N-HSQC spectra, and only a few cross-peaks were observable (Fig. 10). These results indicate that tiny changes in paramagnetic tag introduces additional effects on NMR signals that are further augmented by paramagnetic ions, suggesting stringent quality of paramagnetic tags in assessment of protein properties in complex condition.

The distinct visibility of cross-peaks recorded for the proteins site-specifically labeled with paramagnetic lanthanide ions in diverse crowding media indicates that proteins can interact transiently with the crowding media, and these weak or non-specific interactions cause line-broadening effects. These non-specific associations of proteins with crowding media or cellular components are challenging for the current in-situ NMR study, because any formation of transient encountering complex increases the linewidths of NMR signals. Our data clearly indicated that the additional methyl group in pyridine introduces significant line-broadening effects on ubiquitin S57C-6M-PyDTTA-Ln complex in crowding media, which is in great contrast to the in-vitro experiment.

## Conclusions

In summary, we report two new DTPA-like paramagnetic tags, 4PS-PyDTTA and 4PS-6M-PyDTTA that are readily attached to the solvent exposed cysteine in formation of a stable protein-tag adduct via a thioether bond. The protein-PyDTTA or 6M-PyDTTA adducts show high binding affinities for lanthanide ions, the stability and rigidity of metal complex is tunable by the presence of a methyl group in pyridine. The potential non-specific associations of paramagnetic-tag-Ln complex with protein surface has been evaluated by PREs and the results showed that the 4PS-PyDTTA and 4PS-6M-PyDTTA are high-quality

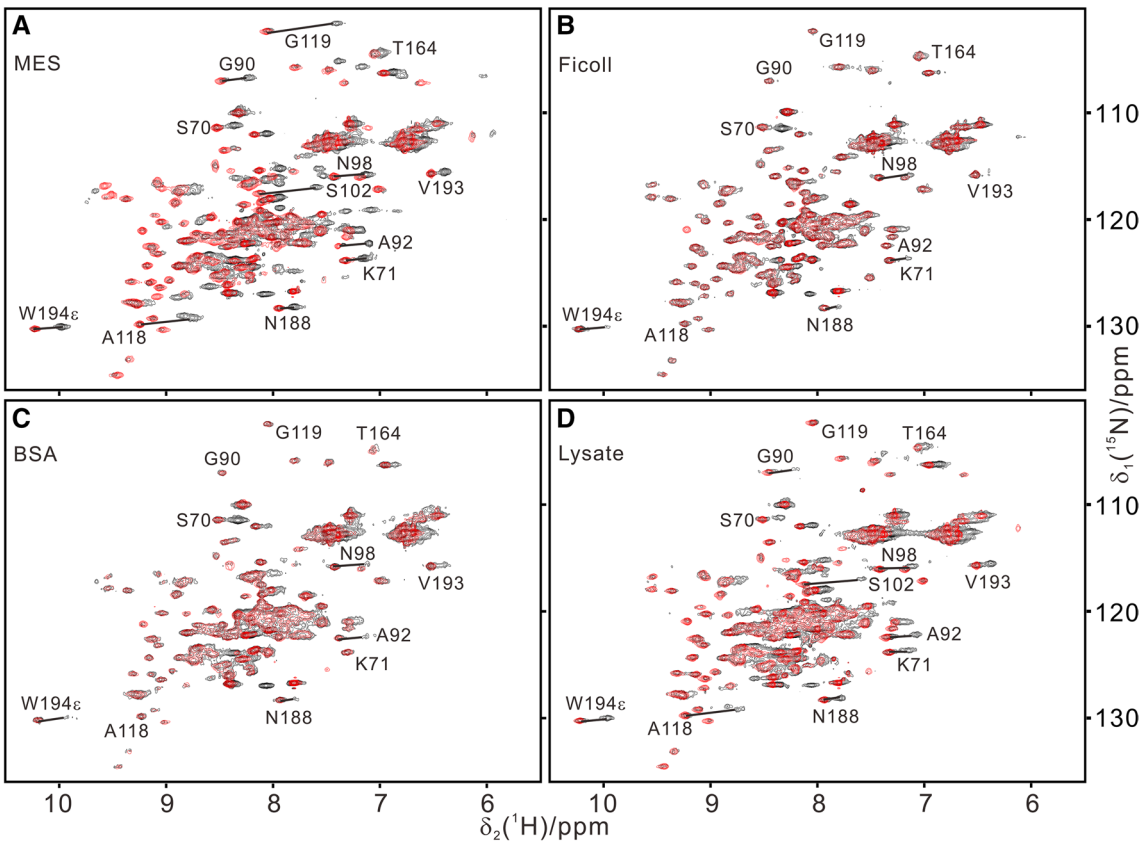


**Fig. 10** Superimposition of $^{15}$N-HSQC spectra recorded for 0.15 mM $^{15}$N-SrtA D82C-6M-PyDTTA (red) and complexed with one equivalent of $Tb^{3+}$ (black) in different crowding media. **a** 20 mM MES buffer at pH 6.4; **b** 200 g/L Ficoll; **c** 100 g/L BSA; **d** *E. coli* cell lysate

PRE tags and the protein-tag-Gd(III) complex produced authentic and reliable PRE effects on proteins that tightly correlated the distance of backbone amide protons from the paramagnetic center.

The application of DTPA-like tags in in-situ NMR analysis of protein was assessed in three different crowding media including Ficoll, BSA and *E. coli* cell lysate. These results indicated that paramagnetic NMR spectroscopy is sensitive to elucidate the dynamics of proteins in in-situ conditions. In addition, cautions must be taken in evaluation of the paramagnetic effects with respect to the crowding media as distinct line-broadening effects are determined in different crowding media. Therefore, stringent quality of paramagnetic tags suitable for paramagnetic NMR analysis of proteins in in-situ condition is highly demanding.

**Acknowledgements** This work was supported by the National Key R&D Program of China (2016YFA0501202) and the Natural Science Foundation of China (21673122 and 21473095).

## References

Anderson MA, Shim H, Raushel FM, Cleland WW (2001) Hydrolysis of phosphotriesters: determination of transition states in parallel reactions by heavy-atom isotope effects. J Am Chem Soc 123:9246–9253

Barbieri L, Luchinat E, Banci L (2016) Characterization of proteins by in-cell NMR spectroscopy in cultured mammalian cells. Nat Protoc 11:1101–1111

Bertini I, Luchinat C, Parigi G (2002) Magnetic susceptibility in paramagnetic NMR. Prog Nucl Magn Reson Spectrosc 40:249–273

Bertini I, Del Bianco C, Gelis I, Katsaros N, Luchinat C, Parigi G, Peana M, Provenzani A, Zoroddu MA (2004) Experimentally exploring the conformational space sampled by domain reorientation in calmodulin. Proc Natl Acad Sci USA 101:6841–6846

Bertini I, Giachetti A, Luchinat C, Parigi G, Petoukhov MV, Pierattelli R, Ravera E, Svergun DI (2010) Conformational space of flexible biological macromolecules from average data. J Am Chem Soc 132:13553–13558

Bertini I, Luchinat C, Nagulapalli M, Parigi G, Ravera E (2012) Paramagnetic relaxation enhancement for the characterization of the conformational heterogeneity in two-domain proteins. Phys Chem Chem Phys 14:9149–9156

Camilloni C, Vendruscolo M (2015) Using pseudocontact shifts and residual dipolar couplings as exact NMR restraints for the determination of protein structural ensembles. Biochemistry 54:7470–7476

Cao C, Chen JL, Yang Y, Huang F, Otting G, Su XC (2014) Selective $^{15}$N-labeling of the side-chain amide groups of asparagine and glutamine for applications in paramagnetic NMR spectroscopy. J Biomol NMR 59:251–261

Chen JL, Wang X, Yang F, Cao C, Otting G, Su XC (2016a) 3D structure determination of an unstable transient enzyme intermediate by paramagnetic NMR spectroscopy. Angew Chem Int Ed 55:13744–13748

Chen JL, Yang Y, Zhang LL, Liang H, Huber T, Su XC, Otting G (2016b) Analysis of the solution conformations of T4 lysozyme by paramagnetic NMR spectroscopy. Phys Chem Chem Phys 18:5850–5859

Clore GM, Iwahara J (2009) Theory, practice, and applications of paramagnetic relaxation enhancement for the characterization of transient low-population states of biological macromolecules and their complexes. Chem Rev 109:4108–4139

Ding Y, Zhao W, Song W, Zhao Z, Ma B (2011) Mild and recyclable catalytic oxidation of pyridines to N-oxides with $H_2O_2$ in water mediated by a vanadium-substituted polyoxometalate. Green Chem 13:1486–1489

Dosset P, Hus JC, Marion D, Blackledge M (2001) A novel interactive tool for rigid-body modeling of multi-domain macromolecules using residual dipolar couplings. J Biomol NMR 20:223–231

Fragai M, Luchinat C, Parigi G, Ravera E (2013) Conformational freedom of metalloproteins revealed by paramagnetism-assisted NMR. Coord Chem Rev 257:2652–2667

Gaponenko V, Altieri AS, Li J, Byrd RA (2002) Breaking symmetry in the structure determination of (large) symmetric protein dimers. J Biomol NMR 24:143–148

Graham B, Loh CT, Swarbrick JD, Ung P, Shin J, Yagi H, Jia X, Chhabra S, Barlow N, Pintacuda G, Huber T, Otting G (2011) DOTA-amide lanthanide tag for reliable generation of pseudocontact shifts in protein NMR spectra. Bioconjugate Chem 22:2118–2125

Guan JY, Keizers PH, Liu WM, Löhr F, Skinner SP, Heeneman EA, Schwalbe H, Ubbink M, Siegal G (2013) Small-molecule binding sites on proteins established by paramagnetic NMR spectroscopy. J Am Chem Soc 135:5859–5868

Hänsel R, Luh LM, Corbeski I, Trantirek L, Dötsch V (2014) In-cell NMR and EPR spectroscopy of biomacromolecules. Angew Chem Int Ed 53:10300–10314

Hass MAS, Ubbink M (2014) Structure determination of protein–protein complexes with long-range anisotropic paramagnetic NMR restraints. Curr Opin Struct Biol 24:45–53

Häussinger D, Huang JR, Grzesiek S (2009) DOTA-M8: an extremely rigid, high-affinity lanthanide chelating tag for PCS NMR spectroscopy. J Am Chem Soc 131:14761–14767

Hikone Y, Hirai G, Mishima M, Inomata K, Ikeya T, Arai S, Shirakawa M, Sodeoka M, Ito Y (2016) A new carbamidemethyl-linked lanthanoid chelating tag for PCS NMR spectroscopy of proteins in living HeLa cells. J Biolmol NMR 66:99–110

Ikegami T, Verdier L, Sakhaii P, Grimme S, Pescatore B, Saxena K, Fiebig KM, Griesinger C (2004) Novel techniques for weak alignment of proteins in solution using chemical tags coordinating lanthanide ions. J Biomol NMR 29:339–349

Jiang WX, Gu XH, Dong X, Tang C (2017) Lanthanoid tagging via an unnatural amino acid for protein structure characterization. J Biolmol NMR 67:273–282

John M, Pintacuda G, Park AY, Dixon NE, Otting G (2006) Structure determination of protein–ligand complexes by transferred paramagnetic shifts. J Am Chem Soc 128:12910–12916

Keizers PHJ, Desreux JF, Overhand M, Ubbink M (2007) Increased paramagnetic effect of a lanthanide protein probe by two-point attachment. J Am Chem Soc 29:9292–9293

Keizers PHJ, Saragliadis A, Hiruma Y, Overhand M, Ubbink M (2008) Design, synthesis, and evaluation of a lanthanide chelating protein probe: CLaNP-5 yields predictable paramagnetic effects independent of environment. J Am Chem Soc 130:14802–14812

Kmentova I, Sutherland HS, Palmer BD, Blaser A, Franzblau SG, Wang B, Wang Y, Ma Z, Denny WA, Thompson AM (2010) Synthesis and structure–activity relationships of aza- and diazabiphenyl analogues of the antitubercular drug (6S)-2-nitro-6-{[4-(trifluoromethoxy)benzyl]oxy}-6,7-dihydro-5H-imidazo[2,1-b][1,3]oxazine (PA-824). J Med Chem 53:8421–8439

Koehler J, Meiler J (2011) Expanding the utility of NMR restraints with paramagnetic compounds: background and practical aspects. Prog Nucl Magn Reson Spectrosc 59:360–389

Lange OF, Lakomek NA, Farès C, Schröder GF, Walter KFA, Becker S, Meiler J, Grubmüller H, Griesinger C, de Groot BL (2008) Recognition dynamics up to microseconds revealed from an RDC-derived ubiquitin ensemble in solution. Science 320:1471–1475

Lee MD, Loh CT, Shin J, Chhabra S, Dennis ML, Otting G, Swarbrick JD, Graham B (2015) Compact, hydrophilic, lanthanide-binding tags for paramagnetic NMR spectroscopy. Chem Sci 6:2614–2624

Leonov A, Voigt B, Rodriguez-Castañeda F, Sakhaii P, Griesinger C (2005) Convenient synthesis of multifunctional EDTA-based chiral metal chelates substituted with an *S*-mesylcysteine. Chem Eur J 11:3342–3348

Li C, Liu M (2012) Protein dynamics in living cells studied by in-cell NMR spectroscopy. FEBS Lett 587:1008–1011

Li QF, Yang Y, Maleckis A, Otting G, Su XC (2012) Thiol–ene reaction: a versatile tool in site-specific labelling of proteins with chemically inert tags for paramagnetic NMR. Chem Commun 48:2704–2706

Liu WM, Keizers PHJ, Hass MAS, Blok A, Timmer M, Sarris AJC, Overhand M, Ubbink M (2012) A pH sensitive, colorful, lanthanide-chelating paramagnetic NMR probe. J Am Chem Soc 134:17306–17313

Liu WM, Overhand M, Ubbink M (2014a) The application of paramagnetic lanthanoid ions in NMR spectroscopy on proteins. Coord Chem Rev 273:2–12

Liu WM, Skinner SP, Timmer M, Blok A, Hass MAS, Filippov DV, Overhand M, Ubbink M (2014b) A two-armed lanthanoid-chelating paramagnetic NMR probe linked to proteins via thioether linkages. Chem Eur J 20:6256–6258

Loh CT, Ozawa K, Tuck KL, Barlow N, Huber T, Otting G, Graham B (2013) Lanthanide tags for site-specific ligation to an unnatural amino acid and generation of pseudocontact shifts in proteins. Bioconjug Chem 24:260–268

Loh CT, Graham B, Abdelkader EH, Tuck KL, Otting G (2015) Generation of pseudocontact shifts in proteins with lanthanides using small "clickable" nitrilotriacetic acid and iminodiacetic acid tags. Chem Eur J 21:5084–5092

Luchinat C (2016) Exploring the conformational heterogeneity of biomolecules: theory and experiments. Phys Chem Chem Phys 18:5684–5685

Luchinat E, Banci L (2016) A unique tool for cellular structural biology: in-cell NMR. J Biol Chem 291:3776–3784

Luchinat E, Banci L (2017) In-cell NMR: a topical review. IUCrJ 4:108–118

Ma FH, Chen JL, Li QF, Zuo HH, Huang F, Su XC (2014) Kinetic assay of the michael addition-like thiol–ene reaction and Insight into protein bioconjugation. Chem Asian J 9:1808–1816

Maltsev A, Grishaev A, Roche J, Zasloff M, Bax A (2014) Improved cross validation of a static ubiquitin structure derived from high precision residual dipolar couplings measured in a drug based liquid crystalline phase. J Am Chem Soc 136:3752–3755

Marley J, Lu M, Bracken C (2001) A method for efficient isotopic labeling of recombinant proteins. J Biomol NMR 20:71–75

Martorana A, Bellapadrona G, Feintuch A, Gregorio ED, Aime S, Goldfarb D (2014) Probing protein conformation in cells by EPR distance measurements using $Gd^{3+}$ spin labeling. J Am Chem Soc 136:13458–13465

Martorana A, Yang Y, Zhao Y, Li QF, Su XC, Goldfarb D (2015) Mn(II) tags for DEER distance measurements in proteins via C–S attachment. Dalton Trans 44:20812–20816

Miranda C, Escartí F, Lamarque L, Yunta MJ, Navarro P, García-España E, Jimeno ML (2004) New 1 H-pyrazole-containing polyamine receptors able to complex l-glutamate in water at physiological pH values. J Am Chem Soc 126:823–833

Müntener T, Häussinger D, Selenko P, Theillet FX (2016) In-cell protein structures from 2D NMR experiments. J Phys Chem Lett 7:2821–2825

Nitsche C, Otting G (2017a) Pseudocontact shifts in biomolecular NMR using paramagnetic metal tags. Prog Nucl Magn Reson Spectrosc 98:20–49

Nitsche C, Mahawaththa MC, Becker W, Huber T, Otting G (2017b) Site-selective tagging of proteins by pnictogen-mediated self-assembly. Chem Commun 53:10894–10897

Ochiai E (1953) Recent Japanese work on the chemistry of pyridine 1-oxide and related compounds. J Org Chem 18:534–551

Ottiger M, Delaglio F, Bax A (1998) Measurement of J and dipolar couplings from simplified two-dimensional NMR spectra. J Magn Reson 131:373–378

Otting G (2010) Protein NMR using paramagnetic ions. Annu Rev Biophys 39:387–405

Pan BB, Yang F, Ye Y, Wu Q, Li C, Huber T, Su XC (2016) 3D structure determination of a protein in living cells using paramagnetic NMR spectroscopy. Chem Commun 52:10237–10240

Pellegatti L, Zhang J, Drahos B, Villette S, Suzenet F, Guillaumet G, Petoud S, Tóth É (2008) Pyridine-based lanthanide complexes: towards bimodal agents operating as near infrared luminescent and MRI reporters. Chem Commun 28:6591–6593

Perica T, Chothia C (2010) Ubiquitin—molecular mechanisms for recognition of different structures. Curr Opin Struct Biol 20:367–376

Peters F, Maestre-Martinez M, Leonov A, Kovačič L, Becker S, Boelens R, Griesinger C (2011) Cys-Ph-TAHA: a lanthanide binding tag for RDC and PCS enhanced protein NMR. J Biomol NMR 51:329–337

Pettit LD, Powell KJ (1999) IUPAC stability constants database, version 4.11. Academic Software, Yorks

Pintacuda G, Park AY, Keniry MA, Dixon NE, Otting G (2006) Lanthanide labeling offers fast NMR approach to 3D structure determinations of protein-protein complexes. J Am Chem Soc 128:3696–3702

Pintacuda G, John M, Su XC, Otting G (2007) NMR structure determination of protein-ligand complexes by lanthanide labeling. Acc Chem Res 40:206–212

Plitzko JM, Schuler B, Selenko P (2017) Structural biology outside the box-inside the cell. Curr Opin Struct Biol 46:110–121

Prudêncio M, Rohovec J, Peters JA, Tocheva E, Boulanger MJ, Murphy ME, Hupkes HJ, Kosters W, Impagliazzo A, Ubbink M (2004) A caged lanthanide complex as a paramagnetic shift agent for protein NMR. Chem Eur J 10:3252–3260

Russo L, Maestre-Martinez M, Wolff S, Becker S, Griesinger C (2013) Interdomain dynamics explored by paramagnetic NMR. J Am Chem Soc 135:17111–17120

Saio T, Ogura K, Shimizu K, Yokochi M, Jr Burke TR, Inagaki F (2011) An NMR strategy for fragment-based ligand screening utilizing a paramagnetic lanthanide probe. J Biomol NMR 51:395–408

Saio T, Ogura K, Kumeta H, Kobashigawa Y, Shimizu K, Yokochi M, Kodama K, Yamaguchi H, Tsujishita H, Inagaki F (2015) Ligand-driven conformational changes of MurD visualized by paramagnetic NMR. Sci Rep 5:16685

Sarkar M, Li C, Pielark GJ (2013) Soft interactions and crowding. Biophys Rev 5:187–194

Schmitz C, Stanton-Cook MJ, Su XC, Otting G, Huber T (2008) Numbat: an interactive software tool for fitting $\Delta\chi$-tensors to molecular coordinates using pseudocontact shifts. J Biolmol NMR 41:179–189

Smith AE, Zhang Z, Pielak GJ, Li C (2015) NMR studies of protein folding and binding in cells and cell-like environments. Curr Opin Struc Biol 30:7–16

Su XC, Otting G (2010) Paramagnetic labelling of proteins and oligonucleotides for NMR. J Biomol NMR 46:101–112

Tang C, Iwahara J, Clore GM (2006) Visualization of transient encounter complexes in protein–protein association. Nature 444:383–386

Tang C, Schwieters CD, Clore GM (2007) Open-to-closed transition in apo maltose-binding protein observed by paramagnetic NMR. Nature 449:1078–1082

Wang J, Zhao J, Zhang X, Gao J (2000) Synthesis and structural determination of nine-coordinate $K_2$ [Y(dtpa)($H_2O$)]†§7$H_2O$. Rare Met 19:241–247

Yang Y, Li QF, Cao C, Huang F, Su XC (2013) Site-specific labeling of proteins with a chemically stable, high-affinity tag for protein study. Chem Eur J 19:1097–1103

Yang Y, Wang JT, Pei YY, Su XC (2015) Site-specific tagging proteins via a rigid, stable and short thiolether tether for paramagnetic spectroscopic analysis. Chem Commun 51:2824–2827

Yang F, Wang X, Pan BB, Su XC (2016) Single-armed phenylsulfonated pyridine derivative of DOTA is rigid and stable paramagnetic tag in protein analysis. Chem Commun 52:11535–11538

Yang Y, Yang F, Gong YJ, Chen JL, Goldfarb D, Su XC (2017) A reactive, rigid Gd(III) labeling tag for in-cell EPR distance measurements in proteins. Angew Chem Int Ed 56:2914–2918

Ye Y, Liu X, Xu G, Liu M, Li C (2015) Direct observation of $Ca^{2+}$-induced calmodulin conformational transitions in Intact *Xenopus laevis* oocytes by $^{19}F$ NMR spectroscopy. Angew Chem Int Ed 54:5328–5330

Yuan Y, Guo S (2011) A mild and efficient synthesis of aryl sulfones from aryl chlorides and sulfinic acid salts using microwave heating. Synlett 18:2750–2756

Zong Y, Bice TW, Ton-That H, Schneewind O, Narayana SV (2004) Crystal structures of *Staphylococcus aureus* sortase A and its substrate complex. J Biol Chem 279:31383–31389